DOI: https://doi.org/10.15407/pmach2024.04.051

UDC 531

BEHAVIOR OF FUNCTIONALLY GRADED POROUS PLATE IN BENDING WITH SMOOTHED ELEMENT

Lan Hoang Ton-That
tonthathoanglan.247@gmail.com
ORCID: 0000-0002-3544-917X

University of Architecture Ho Chi Minh City
196 Pasteur, Vo Thi Sau Ward, District 3, Ho Chi Minh, Vietnam

The bending analysis of functionally graded porous (FGP) plates using a four-node quadrilateral element connected to the C^0-type of Reddy's third-order shear deformation theory and cell-based smoothed strains is presented in this paper. Reddy's theory surely uses the advantages and desirable properties of third-order shear deformation theory. Moreover, FGP plates with advanced material properties are changed from the bottom to the top surface, respectively. Numerical results and comparisons with other reference solutions indicate the accuracy and efficiency of the current element in the analysis of FGP plates.

***Keywords**: quadrilateral element, C^0-HSDT, FGP material, smoothed strains.*

1. Introduction

These days, excellent mechanical properties combined with multifunctionality and excellent structural implementation are of high demand. Valuable properties of functionally graded structures have been heavily utilized in various engineering applications. However, the internal cavities, or porosity, greatly reduce the stiffness of these structures. To boost the understanding of functionally graded porous structures, this paper is born. One can see many papers by different authors mentioning this type of structure. The paper [1] was aimed to review the recent research advances in this field by centering on the adopted mechanical analysis approaches, the obtained findings, and the application opportunities. The fundamental ideas of FG porous composites and the associated structural forms were first covered in detail by the authors. The widely employed theoretical analysis method was subsequently looked at, touching on the nanofiller reinforcement and followed by the details and examples for numerical modelling and mechanical tests. The related artificial intelligence assisted calculations were also discussed. The fabrication techniques of functionally graded porous specimens, e.g. additive manufacturing, and the foam, lattice, and honeycomb-based studies were strategically categorized. The later performance overview highlights the advantages originated from non-uniform cellular morphologies in the overall buckling, bending, vibration, and compressive energy absorption. In the literature, a scaled boundary finite element method framework was presented for the bending and free vibration analyses of functionally graded porous plates based on the 3D elastic theory [2]. Green's theorem and the virtual work principle were both used to derive the governing equation. Distributions of porosity, both even and uneven, were carried out. By leaving the scaling center at infinity, the 3D plate geometry could be obtained by translating the 2D mesh along the radial direction. As a result, the computational efficiency was greatly increased while the spatial dimension of the model was decreased. Owing to its superior accuracy and convergence, the middle plane of the plate was discretized using the 2D high-order spectral element. Based on a four variable plate theory, the [3] sought to examine the free vibration and bending properties of Levy-type porous functionally graded plate with two opposing simply supported edges. The porosity term in the through-thickness direction was added to the mixture rule to define the material properties of the porous functionally graded plate. The Hamilton principle was used to derive the equations of motion. The porous functionally graded plate's governing equation was found using a state-space approach. Functionally graded plates with 3D random porosity were subjected to static bending and free vibration analyses using a systematic spectral stochastic isogeometric analysis procedure, as described in [4]. The porosity was modeled as a Beta random field, represented compactly via the Karhunen-Loève expansion. A novel hierarchical locking-free quasi-3D shear deformation theory, called spectral displacement formulation, was proposed to approach exact 3D solutions and reflect more realistic effects of the random porosity field. Isogeometric analysis was utilized to meet the C^1-continuity requirement of the spectral displacement formula-

tion. The response surfaces of the porous functionally graded plates were constructed non-invasively by the spectral collocation method. A new spectral stochastic post-processing process was developed to evaluate the probability characteristics of the responses and exclude the adverse convergence-in-probability property. Using a commercial finite element program called Ansys, the two-directional graded structure was created in paper [5], and the ensuing deflection responses were discovered. The porosity within the graded structure taking into account an even distribution pattern was also included in the model. Using the batch input technique, this model was created by following the basic steps that are available in the Ansys platform. According to the comparative analysis, this simulation model's efficiency allowed it to determine the deflection responses while maintaining accuracy and exhibiting negligible variation from the available data. The bending responses of porous functionally graded thick rectangular plates were studied using a high-order shear deformation theory, as stated in [6]. Since this theory took into account both the effects of shear strain and normal deformation, it did not require a shear correction factor. The porous functionally graded plates were used to derive the equilibrium equations. Next, Navier's technique was applied to derive the solution to the problem. In [7], the propagation properties of flexural edge waves in a thermally-exposed functionally graded poroelastic plate were studied. In order to examine the dynamics of edge waves bending, a transversely isotropic, functionally graded porous material plate supported by a Pasternak elastic foundation was introduced. The displacement field and temperature distributions on the plate were studied using the Moore-Gibson-Thompson thermoelasticity theory and Kirchhoff plate theory, respectively. This study compared edge wave behavior in various porous structures, etc., by testing seven different porosity models. Besides the traditional finite element method, the smoothed finite element method has shown many outstanding features described in the literature [8–10], especially the smoothed element related to the cell-based smoothed strategy that will be presented in this paper. This strategy is easily implemented in the finite element procedure by smoothing the strains on the sub-domains. Moreover, the elements and their sub-domains can be found using this method with little computational overhead.

Returning to FSDT with explicit mentions, the weak-form equations require only the first derivative of the displacement field, whereas the finite element formulation requires only C^0 continuous shape functions. However, shear locking can be managed with reduced integration and happens when the plate's thickness-to-length ratio progressively approaches zero. We understand that the higher-order shear deformation theory (HSDT) is widely utilized because it provides precise transverse shear stresses without the need for shear correction factors. However, the requirement of C^1-continuous approximation for the displacement fields in the higher-order shear deformation theory causes some obstacles when dealing with low-order finite elements, like four-node quadrilateral elements. The HSDT is changed from C^1 to C^0 continuity for displacement fields (C^0-HSDT) in order to address these flaws. This strategy only requests the first derivative of transverse displacements and adds two more variables. For the aforementioned reasons, a smoothed element with four nodes and seven degrees of freedom per node associated with cell-based smoothed strains and the C^0-type of Reddy's third-order shear deformation theory is provided for the FGP plate analysis. The obtained results are completely dependable and free of any undesirable phenomena, as they are based on the application of the C^0-type and high-order shear deformation theory.

This paper is organized as follows: Section 2 provides a brief introduction to the C^0-type of Reddy's third-order shear deformation theory [11, 12], the finite element formulation for plates, and the material properties of functionally graded porous (FGP) plates. In Section 3, a number of numerical examples are thoroughly examined to demonstrate the usefulness of this element in analyzing the bending behavior of FGP plate structure. In Section 4, conclusions are finally drawn.

2. Formulations

Presenting a FGP plate with the geometry shown in Fig. 1 will start the analysis. The symbols "*m*" and "*c*" are metallic and ceramic phase. The mid-plane of the plate is *xy*-plane, while the *z*-axis is perpendicular to the *xy*-plane.

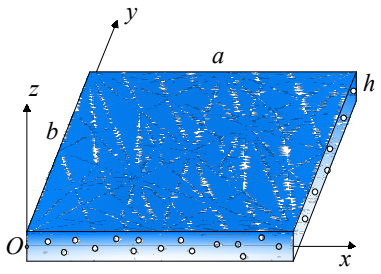

Fig. 1. Configuration of FGP plate

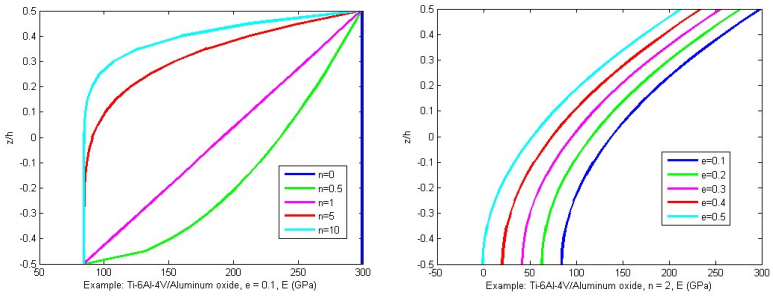

Fig. 2. The modification of E

The modification of E for porosity effect is shown in Fig. 2, which can be expressed as

$$P(z)=(P_c-P_m)\left(\frac{1}{2}+\frac{z}{h}\right)^n+P_m-\frac{e}{2}(P_c+P_m),$$

where P_c and P_m are material properties of ceramic and metallic, n is power-index, and e is porosity. Let Ω be the domain in R^2 occupied by the mid-plane of the plate. The displacement field with 7 unknown variables can be expressed as follows in terms of Reddy's theory C^0-type

$$u(x,y,z)=u_0+\left(z-\frac{4z^3}{3h^2}\right)\phi_x^b-\frac{4z^3}{3h^2}\phi_x^s;$$

$$v(x,y,z)=v_0+\left(z-\frac{4z^3}{3h^2}\right)\phi_y^b-\frac{4z^3}{3h^2}\phi_y^s,\ -\frac{h}{2}\le z\le\frac{h}{2};$$

$$w(x,y,z)=w_0.$$

It is possible to provide the strain-displacement relations in matrix form

$$\begin{Bmatrix}\varepsilon\\ \gamma\end{Bmatrix}=\begin{Bmatrix}\varepsilon^{(0)}\\ \gamma^{(0)}\end{Bmatrix}+z\begin{Bmatrix}\varepsilon^{(1)}\\ 0\end{Bmatrix}+z^2\begin{Bmatrix}0\\ \gamma^{(2)}\end{Bmatrix}+z^3\begin{Bmatrix}\varepsilon^{(3)}\\ 0\end{Bmatrix}$$

with

$$\varepsilon^{(0)}=\begin{Bmatrix}u_{0,x}\\ v_{0,y}\\ u_{0,y}+v_{0,x}\end{Bmatrix};\ \varepsilon^{(1)}=\begin{Bmatrix}\phi_{x,x}^b\\ \phi_{y,y}^b\\ \phi_{x,y}^b+\phi_{y,x}^b\end{Bmatrix};\ \varepsilon^{(3)}=-\frac{4}{3h^2}\begin{Bmatrix}\phi_{x,x}^s+\phi_{x,x}^b\\ \phi_{y,y}^s+\phi_{y,y}^b\\ \phi_{x,y}^s+\phi_{x,y}^b+\phi_{y,x}^b\end{Bmatrix};$$

$$\gamma^{(0)}=\begin{Bmatrix}\phi_y^b+w_{,y}\\ \phi_x^b+w_{,x}\end{Bmatrix};\ \gamma^{(2)}=-\frac{4}{h^2}\begin{Bmatrix}\phi_y^s+\phi_y^b\\ \phi_x^s+\phi_x^b\end{Bmatrix}.$$

The constitutive equations

$$\boldsymbol{\sigma}=\mathbf{D}_m(z)(\boldsymbol{\varepsilon}^{(0)}+z\boldsymbol{\varepsilon}^{(1)}+z^3\boldsymbol{\varepsilon}^{(3)});$$

$$\boldsymbol{\tau}=\mathbf{D}_s(z)(\boldsymbol{\gamma}^{(0)}+z^2\boldsymbol{\gamma}^{(2)})$$

in which

$$\boldsymbol{\sigma}=\begin{bmatrix}\sigma_x & \sigma_y & \sigma_{xy}\end{bmatrix}^{\mathrm{T}};\ \boldsymbol{\tau}=\begin{bmatrix}\tau_{yz} & \tau_{xz}\end{bmatrix}^{\mathrm{T}};$$

$$\mathbf{D}_m(z)=\frac{E(z)}{1-\nu^2(z)}\begin{bmatrix}1 & \nu(z) & 0\\ \nu(z) & 1 & 0\\ 0 & 0 & (1-\nu(z))/2\end{bmatrix};\quad \mathbf{D}_s(z)=\frac{E(z)}{2(1+\nu(z))}\begin{bmatrix}1 & 0\\ 0 & 1\end{bmatrix}.$$

The following matrix form can be used to display the normal and shear forces, bending moments, higher-order values of moments and shear forces

$$\begin{Bmatrix} \mathbf{N} \\ \mathbf{M} \\ \mathbf{P} \\ \mathbf{Q} \\ \mathbf{R} \end{Bmatrix} = \begin{bmatrix} \mathbf{A} & \mathbf{B} & \mathbf{E} & \mathbf{0} & \mathbf{0} \\ \mathbf{B} & \mathbf{D} & \mathbf{F} & \mathbf{0} & \mathbf{0} \\ \mathbf{E} & \mathbf{F} & \mathbf{H} & \mathbf{0} & \mathbf{0} \\ \mathbf{0} & \mathbf{0} & \mathbf{0} & \hat{\mathbf{A}} & \hat{\mathbf{B}} \\ \mathbf{0} & \mathbf{0} & \mathbf{0} & \hat{\mathbf{B}} & \hat{\mathbf{D}} \end{bmatrix} \begin{Bmatrix} \varepsilon^{(0)} \\ \varepsilon^{(1)} \\ \varepsilon^{(3)} \\ \gamma^{(0)} \\ \gamma^{(2)} \end{Bmatrix} = \begin{bmatrix} \mathbf{D_1} & \mathbf{0} \\ \mathbf{0} & \mathbf{D_2} \end{bmatrix} \begin{Bmatrix} \varepsilon^{(0)} \\ \varepsilon^{(1)} \\ \varepsilon^{(3)} \\ \gamma^{(0)} \\ \gamma^{(2)} \end{Bmatrix}$$

with

$$(\mathbf{A},\mathbf{B},\mathbf{D}) = \int_{-h/2}^{h/2} (1, z, z^2) D_m(z) dz \; ; \; (\mathbf{E},\mathbf{F},\mathbf{H}) = \int_{-h/2}^{h/2} (z^3, z^4, z^6) D_m(z) dz \; ; \; (\hat{\mathbf{A}},\hat{\mathbf{B}},\hat{\mathbf{D}}) = \int_{-h/2}^{h/2} (1, z^2, z^4) D_s(z) dz \; .$$

A weak form of the plates can be provided for the static analysis as

$$\int_{\Omega} \delta\boldsymbol{\varepsilon}^{\mathrm{T}} \mathbf{D}_1 \varepsilon d\Omega + \int_{\Omega} \delta\boldsymbol{\gamma}^{\mathrm{T}} \mathbf{D}_2 \boldsymbol{\gamma} d\Omega = \int_{\Omega} \delta w p d\Omega \, ,$$

where p is the transverse loading per unit area. The bounded domain $\boldsymbol{\Omega}$ of plates can be discretized into N_c elements, where N_n represents the total number of nodes. The quadrilateral element with four nodes in the standard FEM's displacement field $\mathbf{u}$ can be roughly represented by

$$\mathbf{u} = \sum_{i=1}^{N_n} \begin{bmatrix} N_i & 0 & 0 & 0 & 0 & 0 & 0 \\ 0 & N_i & 0 & 0 & 0 & 0 & 0 \\ 0 & 0 & N_i & 0 & 0 & 0 & 0 \\ 0 & 0 & 0 & N_i & 0 & 0 & 0 \\ 0 & 0 & 0 & 0 & N_i & 0 & 0 \\ 0 & 0 & 0 & 0 & 0 & N_i & 0 \\ 0 & 0 & 0 & 0 & 0 & 0 & N_i \end{bmatrix} \mathbf{q}_i \, .$$

The nodal degrees of freedom of $\mathbf{u}$ connected to the i^{th} node are represented by the shape function, N_i, and the displacement vector, $\mathbf{q}_i$. Rewriting the strain is possible in the following way

$$\boldsymbol{\varepsilon} = \sum_i \left(\sum_{j=1}^{3} \mathbf{B}_j \right) \mathbf{q}_i \; ; \; \boldsymbol{\gamma} = \sum_i \left(\sum_{j=4}^{5} \mathbf{B}_j \right) \mathbf{q}_i \, ,$$

in which

$$\mathbf{B}_1 = \begin{bmatrix} N_{i,x} & 0 & 0 & 0 & 0 & 0 & 0 \\ 0 & N_{i,y} & 0 & 0 & 0 & 0 & 0 \\ N_{i,y} & N_{i,x} & 0 & 0 & 0 & 0 & 0 \end{bmatrix}; \; \mathbf{B}_2 = \begin{bmatrix} 0 & 0 & 0 & 0 & 0 & N_{i,x} & 0 \\ 0 & 0 & 0 & 0 & 0 & 0 & N_{i,y} \\ 0 & 0 & 0 & 0 & 0 & N_{i,y} & N_{i,x} \end{bmatrix};$$

$$\mathbf{B}_3 = -\frac{4}{3h^2} \begin{bmatrix} 0 & 0 & 0 & N_{i,x} & 0 & N_{i,x} & 0 \\ 0 & 0 & 0 & 0 & N_{i,y} & 0 & N_{i,y} \\ 0 & 0 & 0 & N_{i,y} & N_{i,x} & N_{i,y} & N_{i,x} \end{bmatrix};$$

$$\mathbf{B}_4 = \begin{bmatrix} 0 & 0 & N_{i,y} & 0 & 0 & 0 & N_i \\ 0 & 0 & N_{i,x} & 0 & 0 & N_i & 0 \end{bmatrix}; \; \mathbf{B}_5 = -\frac{4}{h^2} \begin{bmatrix} 0 & 0 & 0 & 0 & N_i & 0 & N_i \\ 0 & 0 & 0 & N_i & 0 & N_i & 0 \end{bmatrix}.$$

From the cell-based smoothed strains strategy [8–10], which transforms the numerical integration from the surfaces to boundary lines of the sub-domains, a quadrilateral element domain Ω_C is further divided into n_C smoothing cells as in Fig. 3. The generalized strain field is smoothed by a weighted average of the original generalized strains using the strain smoothing operation for each smoothing cell

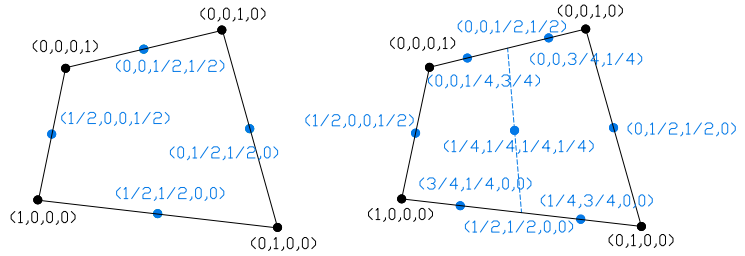

Fig. 3. A quadrilateral element's division into n_C=1 or 2 cells and the shape function values at nodes

$$\bar{\boldsymbol{\varepsilon}}(x_C)=\int_{\Omega_C}\varepsilon(x)\Phi(x-x_C)\,d\Omega\,. \tag{26}$$

The divergence theorem-based smoothed strain can be obtained with

$$\overline{\mathbf{B}}_1=\frac{1}{A_C}\sum_{m=1}^{4}\begin{bmatrix} N_i(x^G)n_x & 0 & 0&0&0&0&0\\ 0 & N_i(x^G)n_y & 0&0&0&0&0\\ N_i(x^G)n_y & N_i(x^G)n_x & 0&0&0&0&0\end{bmatrix}l^C;$$

$$\overline{\mathbf{B}}_2=\frac{1}{A_C}\sum_{b=1}^{4}\begin{bmatrix} 0&0&0&0&0&N_i(x^G)n_x & 0\\ 0&0&0&0&0&0 & N_i(x^G)n_y\\ 0&0&0&0&0&N_i(x^G)n_x & N_i(x^G)n_x\end{bmatrix}l^C;$$

$$\overline{\mathbf{B}}_3=-\frac{4}{3h^2}\sum_{b=1}^{4}\begin{bmatrix} 0&0&0&N_i(x^G)n_x & 0 & N_i(x^G)n_x & 0\\ 0&0&0&0 & N_i(x^G)n_y & 0 & N_i(x^G)n_y\\ 0&0&0&N_i(x^G)n_y & N_i(x^G)n_x & N_i(x^G)n_y & N_i(x^G)n_x\end{bmatrix}l^C.$$

x^G and l^C are the Gauss point and the length of each line segment of the boundary.

The smoothed element stiffness is then given

$$\overline{\mathbf{K}}=\sum_{C=1}^{n_C=1}\overline{\mathbf{B}}_1^{\mathrm{T}}\mathbf{A}\overline{\mathbf{B}}_1+\sum_{C=1}^{n_C=2}(\overline{\mathbf{B}}_1^{\mathrm{T}}\mathbf{B}\overline{\mathbf{B}}_2+\overline{\mathbf{B}}_1^{\mathrm{T}}\mathbf{E}\overline{\mathbf{B}}_3+\overline{\mathbf{B}}_2^{\mathrm{T}}\mathbf{B}\overline{\mathbf{B}}_1+\overline{\mathbf{B}}_2^{\mathrm{T}}\mathbf{D}\overline{\mathbf{B}}_2+\overline{\mathbf{B}}_2^{\mathrm{T}}\mathbf{F}\overline{\mathbf{B}}_3+\overline{\mathbf{B}}_3^{\mathrm{T}}\mathbf{E}\overline{\mathbf{B}}_1+\overline{\mathbf{B}}_3^{\mathrm{T}}\mathbf{F}\overline{\mathbf{B}}_2+\overline{\mathbf{B}}_3^{\mathrm{T}}\mathbf{H}\overline{\mathbf{B}}_3)+$$
$$+\int_{\Omega_C}(\mathbf{B}_4^{\mathrm{T}}\hat{\mathbf{A}}\mathbf{B}_4+\mathbf{B}_4^{\mathrm{T}}\hat{\mathbf{B}}\mathbf{B}_5+\mathbf{B}_5^{\mathrm{T}}\hat{\mathbf{B}}\mathbf{B}_4+\mathbf{B}_5^{\mathrm{T}}\hat{\mathbf{D}}\mathbf{B}_5)\,d\Omega$$

For static analysis

$$\overline{\mathbf{K}}\mathbf{q}=\mathbf{F}$$

with

$$\mathbf{F}=\int_{\Omega_C}\mathbf{p}\mathbf{N}d\Omega\,.$$

3. Numerical results

The current element is used for simply supported FG plate bending analysis. The simply supported boundary conditions for this procedure: $v_0=w_0=\phi_y^s=\phi_y^b=0$ at x=0, a and $u_0=w_0=\phi_x^s=\phi_x^b=0$ at y=0, b. Table 1 displays the various values. The accuracy of the current analysis is verified by comparing it to other numerical case studies. The following material qualities should be present in the aluminum and alumina FG plate: (aluminum, Al): E_m=70 GPa; ν=0.3 and (alumina, Al_2O_3): E_c=380 GPa; ν=0.3. The normalized parameters $\overline{w}=\frac{10hE_0}{a^2q_0}w\left(\frac{a}{2},\frac{b}{2}\right)$, $\overline{\sigma}_x=\frac{10h^2}{a^2q_0}\sigma_x\left(\frac{a}{2},\frac{b}{2},\frac{h}{2}\right)$, and $\overline{\tau}_{xz}=\frac{h}{aq_0}\tau_{zx}\left(0,\frac{b}{2},0\right)$ are used in this paper. First, for various values of the volume fraction n, the following values are considered for the square FG plate (a/h=10

and a/b=1). Comparisons are made between the current predictions and those derived from the high-order (HSDT), parabolic (PSDT), sinusoidal (SSDT), and first-order (FSDT) shear deformation theories [6]. Table 1 and Fig. 4 demonstrate that, even for thicker plates, the current results are satisfactory when compared to alternative solutions.

As an additional illustration, Tables 2, 3, and 4 provide the results of deflections, axial stresses, and transverse shear stresses for porous FG plates (e=0.1, 0.2, and 0.3), respectively. For varying values of the volume fraction graded factor n, the porosity parameter increases the deflections and transverse shear stresses while decreasing the axial stress.

Table 1. Comparison of the normalized parameters of the FG plate for different n values with e=0

Theory	n	$\overline{w}$	$\overline{\sigma}_x$	$\overline{\tau}_{xz}$
FSDT	Ceramic	0.07791	1.97576	0.15915
PSDT		0.07791	1.99432	0.23857
SSDT		0.07790	1.99550	0.24618
HSDT		0.08122	1.99550	0.24618
Article		0.08040	1.99540	0.24616
FSDT	1	0.19609	0.93765	0.26880
PSDT		0.19604	0.94370	0.33433
SSDT		0.19604	0.94407	0.34103
HSDT		0.19603	0.94407	0.34103
Article		0.19604	0.94405	0.34102
FSDT	2	0.28661	1.36934	0.34892
PSDT		0.28490	1.37662	0.40919
SSDT		0.28479	1.37702	0.41426
HSDT		0.28479	1.37702	0.41426
Article		0.28480	1.37700	0.41424
FSDT	5	0.38402	1.83097	1.83097
PSDT		0.38116	1.83989	0.57337
SSDT		0.38090	1.84026	0.57591
HSDT		0.38090	1.84026	0.57591
Article		0.38104	1.84019	0.57575
FSDT	10	0.40768	1.94564	1.94564
PSDT		0.40799	1.95075	0.69891
SSDT		0.40790	1.95096	0.70450
HSDT		0.40703	1.95703	0.75376
Article		0.40744	1.95669	0.75311
FSDT	Metal	0.41919	1.97576	1.97576
PSDT		0.42164	1.98354	0.19984
SSDT		0.42172	1.98392	0.20359
HSDT		0.42290	1.99550	0.24618
Article		0.42198	1.99540	0.24616

Table 2. Effects of n and e on the normalized deflections in a square FG plate

n	e=0.1	e=0.2	e=0.3
Ceramic	0.08120	0.08481	0.08874
1	0.21875	0.24747	0.28500
2	0.33573	0.40904	0.52404
5	0.47779	0.64169	0.97969
Metal	0.34623	0.29313	0.25410

Table 3. Effects of n and e on the normalized axial stresses in a square FG plate

n	e=0.1	e=0.2	e=0.3
Ceramic	1.99540	1.99540	1.99540
1	0.82121	0.66569	0.46258
2	1.26607	1.10627	0.85583
5	1.80178	1.73702	1.60413
Metal	1.99540	1.99540	1.99540

Table 4. Effects of n and e on the normalized transverse shear stresses in a square FG plate

n	e=0.1	e=0.2	e=0.3
Ceramic	0.24616	0.24616	0.24616
1	0.34762	0.35540	0.36467
2	0.42860	0.44644	0.46954
5	0.61220	0.65851	0.72178
Metal	0.24616	0.24616	0.24616

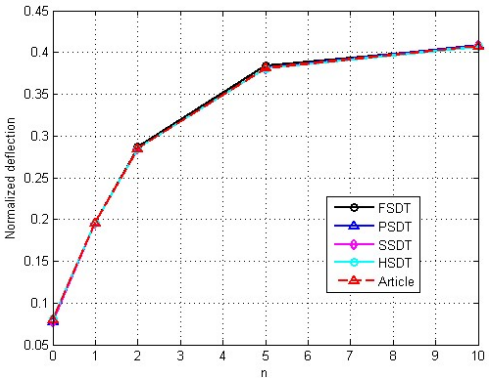

Fig. 4. The comparison of the normalized deflections in a FG plate (a/b=1, a/h=10, e=0

4. Conclusion

A simple model based on the Reddy's theory of high-order shear deformation and cell-based smoothed strains is developed for FGP plates. This theory satisfies the nullity of the stresses at the upper and lower surfaces of the plate without using the shear correction factor. The law of the modified mixture covering the porosity phases provides a rough description of the variations with porosity in the properties of FG plates. The flexion of FGP plates is studied as a function of several parameters, such as gradient index *n* and porosity *e*. Examples are given, and the current model predicts the static analysis of FGP plates with good numerical results.

References

1. Chen, D., Gao, K., Yang, J., & Zhang, L. (2023). Functionally graded porous structures: Analyses, performances, and applications – A Review. *Thin-Walled Structures*, vol. 191, article 111046. https://doi.org/10.1016/j.tws.2023.111046.
2. Yin, Z., Gao, H., & Lin, G. (2021). Bending and free vibration analysis of functionally graded plates made of porous materials according to a novel the semi-analytical method. *Engineering Analysis with Boundary Elements*, vol. 133, pp. 185–199. https://doi.org/10.1016/j.enganabound.2021.09.006.
3. Demirhan, P. A. & Taskin, V. (2019). Bending and free vibration analysis of Levy-type porous functionally graded plate using state space approach. *Composites Part B: Engineering*, vol. 160, pp. 661–676. https://doi.org/10.1016/j.compositesb.2018.12.020.
4. Sun, X., Gao, R., & Zhang, Y. (2023). Spectral stochastic isogeometric analysis of bending and free vibration of porous functionally graded plates. *Applied Mathematical Modelling*, vol. 116, pp. 711–734. https://doi.org/10.1016/j.apm.2022.12.017.
5. Ramteke, P. M., Mahapatra, B. P., Panda, S. K., & Sharma, N. (2020). Static deflection simulation study of 2D Functionally graded porous structure. *Materials Today: Proceedings*, vol. 33, part 8, pp. 5544–5547. https://doi.org/10.1016/j.matpr.2020.03.537.
6. Merdaci, S. & Belghoul, H. (2019). High-order shear theory for static analysis of functionally graded plates with porosities. *Comptes Rendus Mécanique*, vol. 347, no. 3, pp. 207–217. https://doi.org/10.1016/j.crme.2019.01.001.
7. Kumari, T., Som, R., Althobaiti, S., & Manna, S. (2023). Bending wave at the edge of a thermally affected functionally graded poroelastic plate. *Thin-Walled Structures*, vol. 186, article 110719. https://doi.org/10.1016/j.tws.2023.110719.
8. Ton-That, H. L. (2023). Four-node quadrilateral C0-element based on cell-based smoothed strains strategy and third-order shear deformation theory for functionally graded carbon nanotube reinforced composite plates. *Rakenteiden Mekaniikka – Journal of Structural Mechanics*, vol. 56, no. 1, pp. 1–23. https://doi.org/10.23998/rm.119608.
9. Ton-That, H. L., Nguyen-Van, H., & Chau-Dinh, T. (2020). Static and buckling analyses of stiffened plate/shell structures using the quadrilateral element SQ4C. *Comptes Rendus Mécanique*, vol. 348, no. 4, pp. 285–305. https://doi.org/10.5802/crmeca.7.
10. Nguyen-Van, H., Mai-Duy, N., Karunasena, W., & Tran-Cong, T. (2011). Buckling and vibration analysis of laminated composite plate/shell structures via a smoothed quadrilateral flat shell element with in-plane rotations. *Computers & Structures*, vol. 89, iss. 7–8, pp. 612–625. https://doi.org/10.1016/j.compstruc.2011.01.005.
11. Reddy, J. N. (1984). A simple higher-order theory for laminated composite plates. *Journal of Applied Mechanics*, vol. 51, iss. 4, pp. 745–752. https://doi.org/10.1115/1.3167719.
12. Phan, N. D. & Reddy, J. N. (1985). Analysis of laminated composite plates using a higher-order shear deformation theory. *International Journal for Numerical Methods in Engineering*, vol. 21, iss. 12, pp. 2201–2219. https://doi.org/10.1002/nme.1620211207.

Received 19 October 2024

Поведінка функціонально-градієнтної пористої пластини при згині із використанням згладженого елемента

L. H. Ton-That

Архітектурний університет Хошиміна
196 Pasteur, Vo Thi Sau Ward, District 3, м. Хошимін, В'єтнам

У цій статті описується аналіз згину функціонально-градієнтних пористих (ФГП) пластин із використанням чотирикутного елементу з чотирма вузлами, пов'язаного з C^0-типом теорії деформації зсуву третього порядку Редді та комірчастими згладженими деформаціями. Теорія Редді використовує переваги та бажані властивості теорії деформації зсуву третього порядку. Більше того, пластини ФГП з покращеними властивостями

матеріалу змінюються з нижньої поверхні на верхню відповідно. Чисельні результати і порівняння з іншими стандартними розчинами вказують на точність й ефективність поточного елементу при аналізі пластин ФГП.

***Ключові слова**: чотиригранний елемент, C^0-ТДЗВП, матеріал ФГП, згладжені деформації.*

Література

1. Chen D., Gao K., Yang J., Zhang L. Functionally graded porous structures: Analyses, performances, and applications – A Review. *Thin-Walled Structures*ю 2023. Vol. 191. Article 111046. https://doi.org/10.1016/j.tws.2023.111046.
2. Yin Z., Gao H., Lin G. Bending and free vibration analysis of functionally graded plates made of porous materials according to a novel the semi-analytical method. *Engineering Analysis with Boundary Elements*. 2021. Vol. 133. P. 185–199. https://doi.org/10.1016/j.enganabound.2021.09.006.
3. Demirhan P. A., Taskin V. Bending and free vibration analysis of Levy-type porous functionally graded plate using state space approach. *Composites Part B: Engineering*. 2019. Vol. 160. P. 661–676. https://doi.org/10.1016/j.compositesb.2018.12.020.
4. Sun X., Gao R., Zhang Y. Spectral stochastic isogeometric analysis of bending and free vibration of porous functionally graded plates. *Applied Mathematical Modelling*. 2023. Vol. 116. P. 711–734. https://doi.org/10.1016/j.apm.2022.12.017.
5. Ramteke P. M., Mahapatra B. P., Panda S. K., Sharma N. Static deflection simulation study of 2D Functionally graded porous structure. *Materials Today: Proceedings*. 2020. Vol. 33. Part 8. P. 5544–5547. https://doi.org/10.1016/j.matpr.2020.03.537.
6. Merdaci S., Belghoul H. High-order shear theory for static analysis of functionally graded plates with porosities. *Comptes Rendus Mécanique*. 2019. Vol. 347. No. 3. P. 207–217. https://doi.org/10.1016/j.crme.2019.01.001.
7. Kumari T., Som R., Althobaiti S., Manna S. Bending wave at the edge of a thermally affected functionally graded poroelastic plate. *Thin-Walled Structures*. 2023. Vol. 186. Article 110719. https://doi.org/10.1016/j.tws.2023.110719.
8. Ton-That H. L. Four-node quadrilateral C0-element based on cell-based smoothed strains strategy and third-order shear deformation theory for functionally graded carbon nanotube reinforced composite plates. *Rakenteiden Mekaniikka – Journal of Structural Mechanics*. 2023. Vol. 56. No. 1. P. 1–23. https://doi.org/10.23998/rm.119608.
9. Ton-That H. L., Nguyen-Van H., Chau-Dinh T. Static and buckling analyses of stiffened plate/shell structures using the quadrilateral element SQ4C. *Comptes Rendus Mécanique*. 2020. Vol. 348. No. 4. P. 285–305. https://doi.org/10.5802/crmeca.7.
10. Nguyen-Van H., Mai-Duy N., Karunasena W., Tran-Cong T. Buckling and vibration analysis of laminated composite plate/shell structures via a smoothed quadrilateral flat shell element with in-plane rotations. *Computers & Structures*. 2011. Vol. 89. Iss. 7–8. P. 612–625. https://doi.org/10.1016/j.compstruc.2011.01.005.
11. Reddy J. N. A simple higher-order theory for laminated composite plates. *Journal of Applied Mechanics*. 1984. Vol. 51. Iss. 4. P. 745–752. https://doi.org/10.1115/1.3167719.
12. Phan N. D., Reddy J. N. Analysis of laminated composite plates using a higher-order shear deformation theory. *International Journal for Numerical Methods in Engineering*. 1985. Vol. 21. Iss. 12. P. 2201–2219. https://doi.org/10.1002/nme.1620211207.